

Cardiac Electrophysiology Using LS-DYNA[®]

Pierre L'Eplattenier, Iñaki Çaldichoury, Facundo Del Pin,
Rodrigo Paz, Attila Nagy, Dave Benson
Livermore Software LLC

Abstract

Heart disease is among the leading causes of death in the Western world; hence, a deeper understanding of cardiac functioning will provide important insights for engineers and clinicians in treating cardiac pathologies. However, the heart also offers a significant set of unique challenges due to its extraordinary complexity. In this respect, some recent efforts have been made to be able to model the multiphysics of the heart using LS-DYNA.

The model starts with electrophysiology (EP) which simulates the propagation of the cell transmembrane potential in the heart. This electrical potential triggers the onset of cardiac muscle contraction, which then results in the pumping of the blood to the various organs in the body. The EP/mechanical model can be coupled with a Fluid Structure Interaction (FSI) model to study the clinically relevant blood flow parameters as well as valves or cardiac devices. This paper concentrates on the EP part of the model. Other papers in this conference will present the mechanical and FSI parts.

Different propagation models, called "mono-domain" or "bi-domain", which couple the diffusion of the potential along the walls of the heart with ionic equations describing the exchanges between the inner and the outer parts of the cells have been implemented. These models were first benchmarked against published results obtained from other EP research codes on a simple cuboid heart tissue model. More recently, we also performed benchmarks proposed by the FDA against analytical solutions. Other features of the EP solver will also be presented such as coupling between the tissue and a surrounding bath, coupling between mono and bi-domain in the same model, and coupling of the mono/bi domain models with a Purkinje Network.

Finally, multi-physics simulations with the EP coupled with mechanical deformation and FSI for the blood flow will be presented. These models include arteries and valves for a realistic model of a ventricular pump.

1-Introduction

A cardiac computational model can give biomedical researchers an additional source of information to understand how the heart works. Simulation can be the base of theoretical studies into the mechanisms of cardiac pathologies, provide diagnostic value or can be used to assist in therapy planning. The goal of LSTC is to be able to simulate the pumping heart, with a coupling scheme between the EP equations describing the propagation of the transmembrane potential, the mechanical deformations triggered by this electrical potential, and the blood flow in this pumping heart.

Section 2 will present the EP models introduced in LS-DYNA, section 3 will show some benchmarks between LS-DYNA and other EP codes, in section 4, we will show an example of spiral wave development in a ventricle, in section 5 we will present the automatic generation of a Purkinje network and its coupling with the mono and bidomain models, and finally, section 6 will present the coupling of the EP with mechanical deformation and hemodynamics.

2-Presentation of the model

The wall of the heart has three layers: epicardium, myocardium and endocardium. The endocardium and epicardium are thin layers consisting primarily of collagen and elastic tissue. In the middle layer, the myocardium, the cells that constitute the muscle show electrical excitability. These specialized cells, called myocytes, are organized into parallel cardiac fibers giving the muscle the striated appearance. The fibers form sheets which are connected by a collagenous network [1].

A cardiac cell (myocyte) is typically 10 to 20 μm in diameter and 80 to 125 μm in length. The cell membrane acts as an electrical insulator and contains ion channels which transport electrical current by diffusion. The potential difference across the membrane is called the transmembrane potential. Initially, a cardiac cell is at rest, with a potential difference across the membrane. The potential inside the cell is negative compared to the external, with a potential difference around 80mV. If the membrane potential rises to a certain threshold value (close to 40 mV) a rapid process occurs, during which different ions, mainly Na^+ , K^+ , and Ca^{2+} , are exchanged between the inner and the outer part of the cell, creating a fast depolarization, an early repolarization, a plateau and a final repolarization. The complete cycle of depolarization and repolarization lasts around 300 ms and is called “action potential”. It is shown in Figure (1). This action potential diffuses from cell to cell through a network of gap junctions, creating a wave of depolarization and repolarization through the myocardium [1].

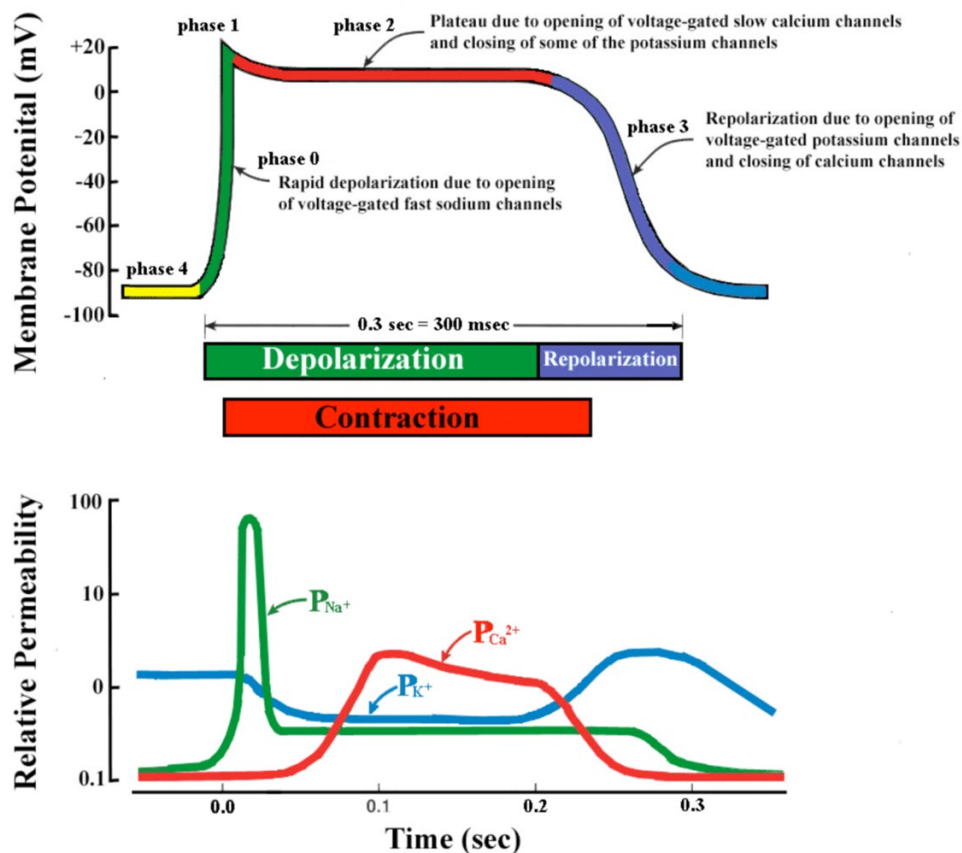


Figure 1: A typical action potential of a ventricular myocyte and the underlying ion currents. The resting membrane potential is approximately ~ 80 mV (phase 4). The rapid depolarization is primarily due to the voltage gated Na^+ current (phase 0), which results in a relatively sharp peak (phase 1) and transitions into the plateau (phase 2) until repolarization (phase 3). Also indicated are the refractory period and timing of the ventricular contraction. Modified from Tortora GJ, Grabowski SR. Principles of Anatomy and Physiology, ninth edition. New York: John Wiley & Sons, Inc., 2000

2-1 The bidomain model

Since describing the whole heart, or even part of it like a ventricle, at the cell level would be computationally too expensive, continuous approximations are made, where the inner part of the cells is treated as one continuum “domain” with an inner potential $\phi_i(\vec{x}, t)$, and the outer part as another domain with an external potential $\phi_e(\vec{x}, t)$. Each domain is characterized by a conductivity tensor, called respectively σ_i and σ_e . These tensors are usually highly non-isotropic, with factors that can be as high as 5 to 10 between the conductivity along the fibers and the one across the fibers. Therefore, it is very important to correctly model the fiber orientation, which can be consumed from an imaging technique called the diffusion tensor MRI. A transmembrane current with surface density I_m flows between the two domains hence the so called “bi-domain” equations [2]:

$$\nabla \cdot (\sigma_i \nabla \phi_i) = \beta I_m \quad (1)$$

$$\nabla \cdot (\sigma_e \nabla \phi_e) = -\beta I_m \quad (2)$$

where β is the membrane surface to volume ratio.

This transmembrane current density I_m consists of a capacitive part, an ionic part generated by the cell membrane I_{ion} , and an imposed stimulation current density I_{stim} :

$$I_m = C_m \frac{\partial V_m}{\partial t} + I_{ion} + I_{stim} \quad (3)$$

where C_m is the membrane capacity per unit area, and we introduced the transmembrane potential:

$$V_m = \phi_i - \phi_e \quad (4)$$

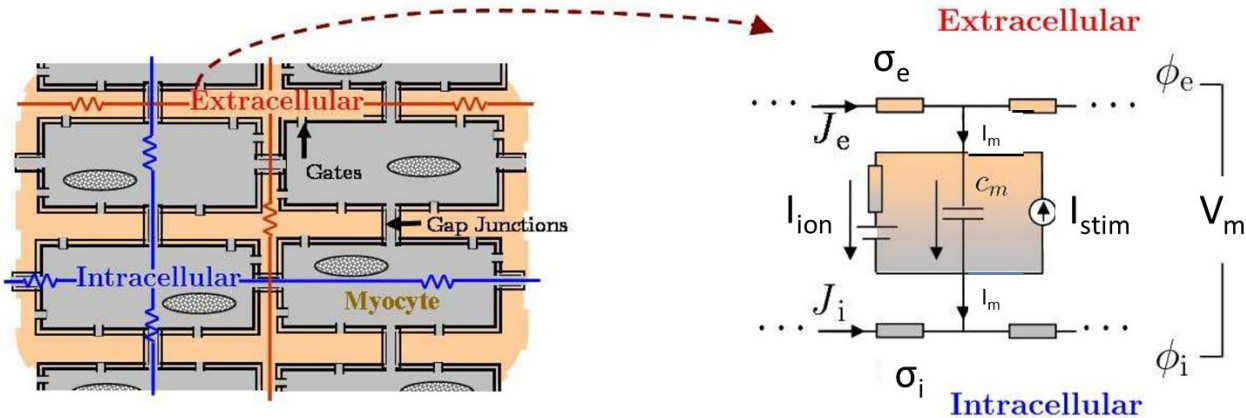


Figure 2: Illustration of the bidomain method (adapted from “Multiscale forward electromagnetic model of uterine contractions during pregnancy”, La Rosa et al. BMC Medical Physics 2012, 12:4.).

Using (3) and (4), we can rewrite equations (1) and (2) in terms of V_m and ϕ_e as:

$$\beta C_m \frac{\partial V_m}{\partial t} + \beta I_{ion}(V_m, \mathbf{u}) - \nabla \cdot (\sigma_i \nabla V_m) - \nabla \cdot (\sigma_i \nabla \phi_e) = \beta I_{stim}(\vec{x}, t) \quad (5)$$

$$\nabla \cdot (\sigma_i \nabla V_m) + \nabla \cdot ((\sigma_i + \sigma_e) \nabla \phi_e) = 0 \quad (6)$$

In equation (5), we wrote $I_{ion}(V_m, \mathbf{u})$, to indicate that the ionic current density depends not only on the transmembrane potential V_m , but also on an extra set of variables that we represent by \mathbf{u} . The number of such variables and their time evolution depend on the cell model chosen, which we write, in a general way:

$$\frac{\partial \mathbf{u}}{\partial t} = f(\mathbf{u}, V_m) \quad (7)$$

These cell models locally describe the exchange of ions through the cell membrane, as schematically shown in Figure 1. Depending upon the question of interest, one can select from a wide class of ionic models, ranging from the FitzHugh-Nagumo model [3][4] with two variables or the Fenton-Karma model with 3 variables [5] to the one discussed in this paper, the ten Tusscher and Panfilov model [6] with 19 variables.

Projecting equations (5) and (6) onto the FEM basis functions, we get:

$$\beta C_m M \frac{\partial V_m}{\partial t} + \beta I_{ion} - S_i V_m - S_i \phi_e = \beta I_{stim} \quad (8)$$

$$S_i V_m - S_{ie} \Phi_e = 0 \quad (9)$$

where

$$M(i, j) = \int_{\Omega} \varphi_i \varphi_j d\Omega \quad (10)$$

Is the mass matrix, and

$$S_i(i, j) = \int_{\Omega} \sigma_i \nabla \varphi_i \cdot \nabla \varphi_j d\Omega \quad (11)$$

and

$$S_{ie}(i, j) = \int_{\Omega} (\sigma_i + \sigma_e) \nabla \varphi_i \cdot \nabla \varphi_j d\Omega \quad (12)$$

are diffusion stiffness matrices corresponding to different conductivities.

In order to solve the coupled diffusion equations (8)-(9) with the ionic one (7), we use a so called ‘‘Spiteri-Ziaratgahi’’ operator splitting [7] where the advance from time t to time $t+1$ reads:

$$u(t+1) = u(t) + dt f(u(t), V_m(t), t) \quad (13)$$

$$\begin{bmatrix} \frac{\beta C_m}{dt} M + S_i & S_i \\ S_i & S_{ie} \end{bmatrix} \cdot \begin{bmatrix} V_m(t+1) \\ \phi_e(t+1) \end{bmatrix} = \begin{bmatrix} \frac{\beta C_m}{dt} M V_m(t) - \beta M I_{ion}(u(t+1), V_m(t), t) + \beta M I_{stim} \\ 0 \end{bmatrix} \quad (14)$$

2-2 The monodomain model

The monodomain model makes the extra hypothesis that the inner and outer conductivity tensors are proportional: $\sigma_e = \lambda \sigma_i$. We introduce a mean conductivity [2]:

$$\sigma = \frac{\sigma_i \sigma_e}{\sigma_i + \sigma_e} \quad (15)$$

or

$$\sigma_i = (1 + \lambda) \sigma \quad (16)$$

$$\sigma_e = \frac{1 + \lambda}{\lambda} \sigma \quad (17)$$

Equation (6) gives:

$$\nabla \cdot (\sigma_i \nabla \phi_e) = -\frac{\lambda}{1 + \lambda} \nabla \cdot (\sigma_i \nabla V_m) \quad (18)$$

which gives, when using it in (5), an equation on V_m only:

$$\beta C_m \frac{\partial V_m}{\partial t} + \beta I_{ion}(V_m, u) - \nabla \cdot (\sigma \nabla V_m) = \beta I_{stim}(\vec{x}, t) \quad (19)$$

This is the monodomain equation.

When projecting equation (19) onto the FEM basis functions, we get:

$$\beta C_m M \frac{\partial V}{\partial t} + \beta I_{ion} - S V = \beta I_{stim} \quad (20)$$

with

$$S(i, j) = \int_{\Omega} \sigma \nabla \varphi_i \cdot \nabla \varphi_j d\Omega \quad (21)$$

And M is defined by (10).

2-3 Coupling with a surrounding bath

It is important to be able to have the tissue surrounded by a perfusing ‘bath’ through which extracellular current can also flow. This surrounding bath can represent either blood for an in-vivo scenario or Tyrode’s solution for in-vitro perfused experimental comparisons. The bath acts as a path for the external current to flow as shown in figure 3. There are no cells hence no internal potential of current in the bath.

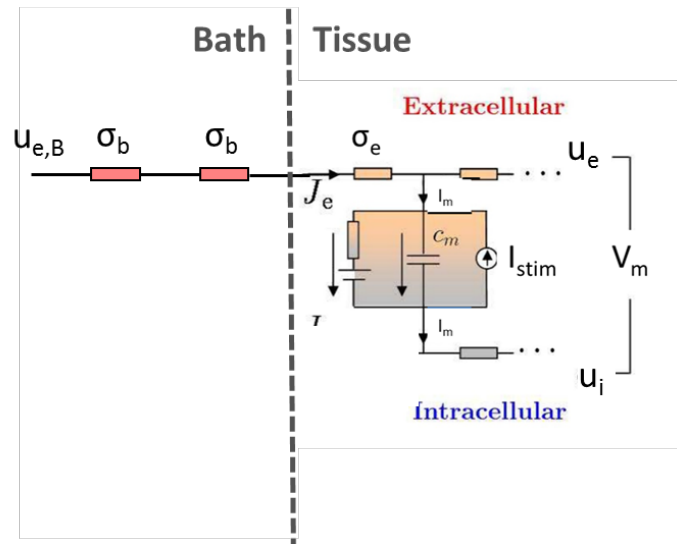


Figure 3: Schematic of the electrical coupling between the tissue with an extra and intra cellular potential and the bath with only the extra-cellular potential

The connection of a bath with a tissue as presented on figure 3 can easily be implemented in the bidomain model where there are degrees of freedom (DOFs) for both the intra and the extra cellular potentials in the tissue, and the connection merely corresponds to adding constraints between the DOFs of the bath potential with the ones of the extracellular potential of the tissue at the boundary bath-tissue, as well as a conservation of the extracellular current.

In the monodomain model, where there are DOFs for the transmembrane potential only, we can use a method called “augmented MonoDoMain Equivalent bidomain model (MDMEQ)”, described in details in [15], where the effect of the bath is represented by an increased conductivity - which depends on the conductivity of the bath, and the intra and extra conductivities of the tissue - as shown in [15] in a thin area surrounding the tissue.

Due to the values of the bath conductivities compared to the ones of the tissue, the bath often creates a shunting effect for the current in the region close to the tissue-bath interface, lowering the effective extracellular resistance by providing a low resistance pathway for current to flow. This so-called bath-loading effect increases the conduction velocity at the tissue surface, relative to the bulk, resulting in a curved transmural profile of the activation wavefront.

This phenomena can be seen in the following model, presented in detail in [15], where a thin 3D slab of tissue of size (3 cm x 0.01 cm x 1cm) is surrounded by a perfusing bath on each side, with an EP wave triggered by an initial transmembrane current pulse at the bottom of the slab, as shown on figure 4.

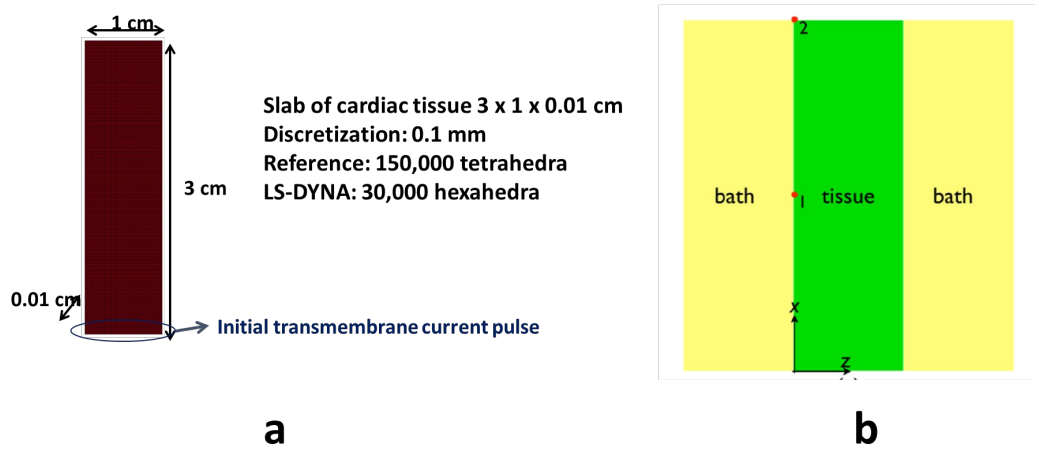


Figure 4: Slab of tissue surrounded by a bath used for the benchmark of LS-DYNA against CARP using the results presented in [15]

The propagation of the EP wave was compared between LS-DYNA and the results of [15] which were obtained using the Cardiac Arrhythmia Research Package (CARP) [16]. This is shown on figure 5. One can see the good agreement between LS-DYNA and CARP, both using the Bidomain (BDM) and the MDMEQ models. One can also see the effect of the surrounding bath curving the wavefront at the bath-tissue boundary.

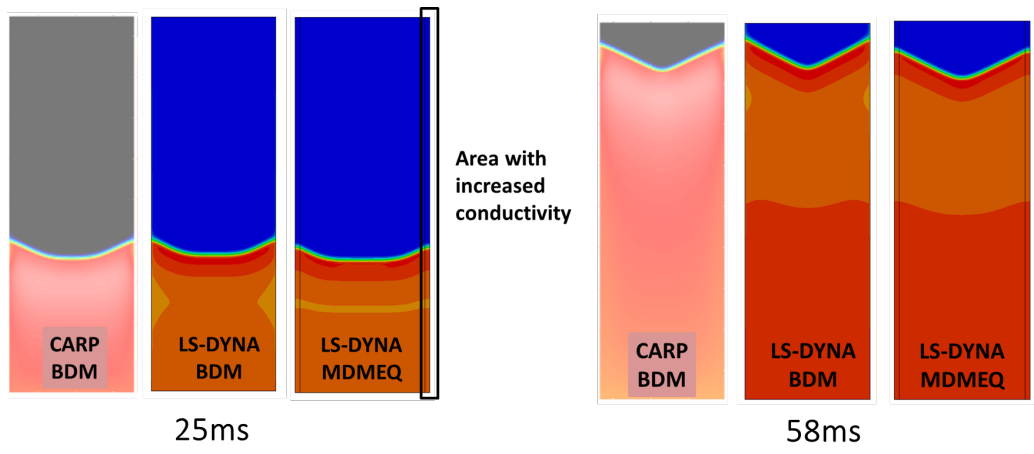


Figure 5: Comparison of the propagation of the EP wave between CARP from [15] and LS-DYNA using both the Bidomain model (BDM) and the extended monodomain model (MDMEQ)

2-4 Monodomain-bidomain and bath coupling

The monodomain model is twice less expensive than bi-domain but is not as reliable in the presence of applied currents (pacing, defibrillation) or in areas with late recovery of the action potential. We thus added the capability to couple the monodomain and bidomain models (as well as a bath) in the same simulation. This is done by solving the monolithic system below, where V^b and V^m represent the bidomain and monodomain transmembrane potentials respectively, and U^b the bidomain extracellular potential.

$$u_{t+1} = u_t + dt f(u_t, V_t, t)$$

$$\begin{bmatrix} \frac{\beta C_m}{dt} M + S_i & S_i & 0 \\ S_i & S_{ie} & 0 \\ 0 & 0 & \frac{\beta C_m}{dt} M + S \end{bmatrix} \begin{bmatrix} V_{t+1}^b \\ U_{t+1}^b \\ V_{t+1}^m \end{bmatrix} = RHS$$

Figure 6 shows a propagation equivalent to the one shown in figure 5, but where the mono-domain was coupled with the bidomain in a small area of the simulation. Even if the propagation is very similar the one using pure mono or pure bidomain models, one can notice the slight deformations of the wave that the coupling between the 2 models generates.

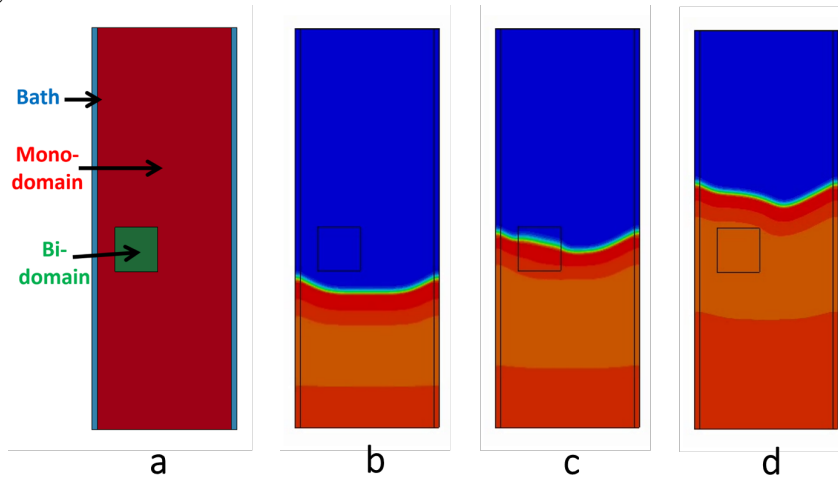


Figure 6: Propagation of the transmembrane potential (b, c, d) in a slab of tissue surrounded by a bath, using the monodomain coupled by the bidomain as shown in (a)

3-FDA Electrophysiology Benchmark

Other benchmarks of the EP were presented in [13]. Here we concentrate on a benchmark proposed in [12] which consists of a cube of cardiac tissue (see figure 7) with a simple enough cell ion model and excitation so that the propagation of the transmembrane potential has an analytical solution. The numerical and analytical solutions can be compared via the computation of a spatio-temporal L2 norm of the difference between the 2 solutions. Figure 8 shows this L2 norm as a function of the mesh density and compares it with the error from the code Chaste (Cancer, Heart and Soft Tissue Environment) [17], which is used in [12]. One can appreciate the tininess of the LS-DYNA error.

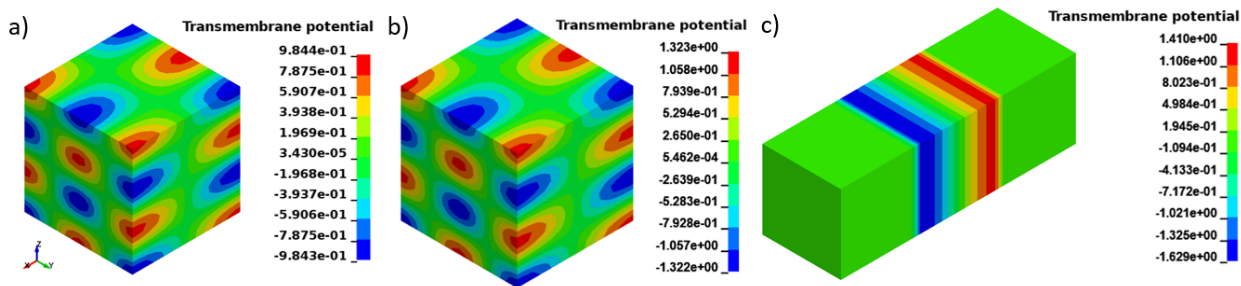


Figure 7: Transmembrane potential distribution at $t=1$ (end time) for a- monodomain, b- bidomain and c- bidomain with bath

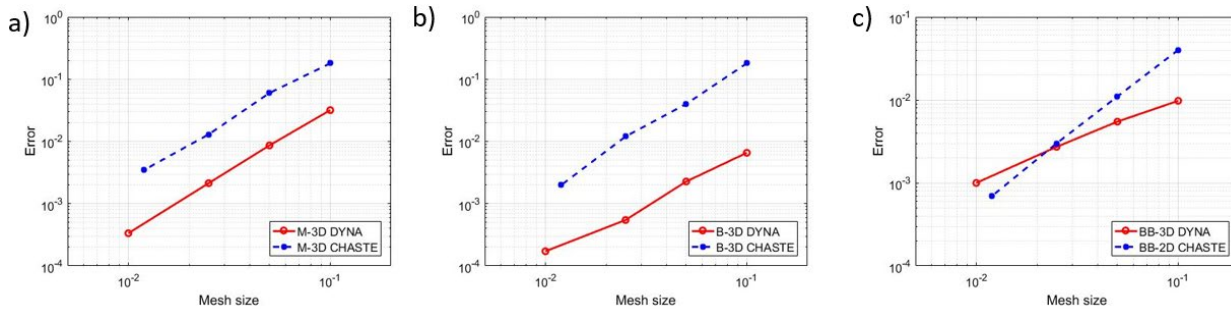


Figure 8: Error between numerical and analytical models vs mesh density with LS-DYNA (red) and Chaste (blue), a) monodomain, b) bidomain, c) bidomain with bath.

4-Spiral waves and arrhythmia in a ventricle

The propagation of electrical waves through cardiac tissue is a very important phenomenon to study since those waves activate the mechanisms for cardiac contraction, responsible to pump blood to the body. In a healthy heart, an electrical wave of action potential propagates in a regular way through the various regions of the heart. Figure 9, which corresponds to a monodomain simulation on a 3D mesh with about 160,000 elements with the size and the shape of a ventricle, and where a stimulus was applied at the bottom, shows such a regular propagation.

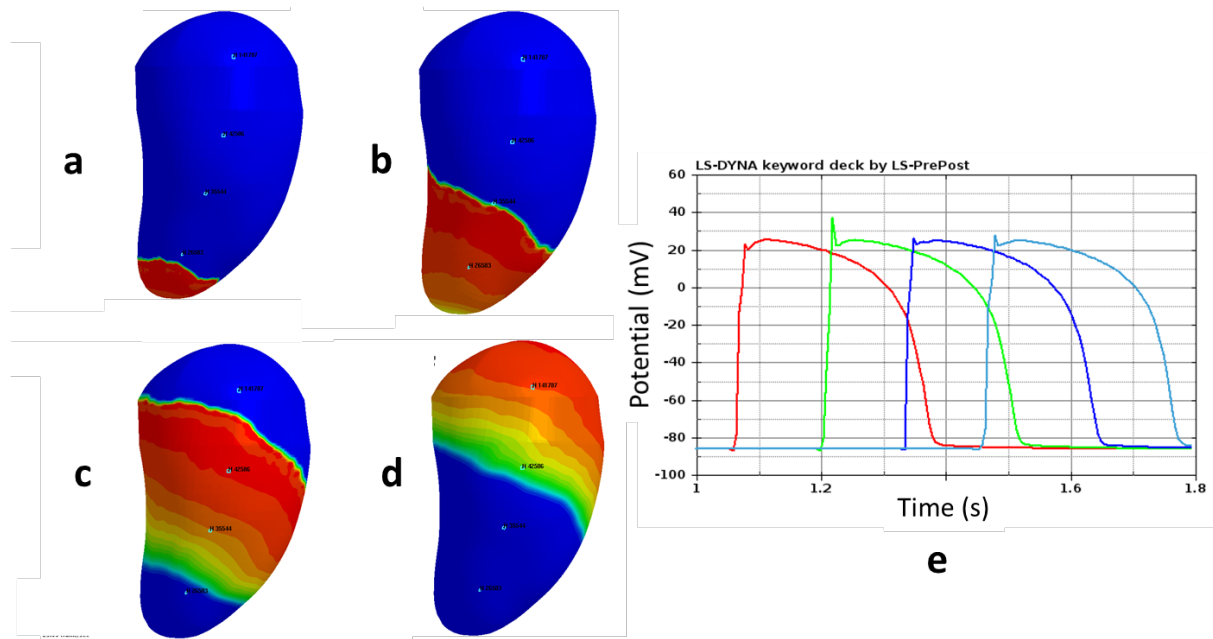


Figure 9: Propagation of the transmembrane potential in a healthy ventricle. The plots on the left show the fringe components of the potential at time 1050 ms (a), 1200 ms (b), 1400 ms (c), and 1600 ms (d). e shows time evolution of the potential at the 4 elements marked on the plots.

One of the proposed mechanisms involved in the development of certain type of arrhythmias are spiral waves, which are symptomatic of functional reentry [6]. Spiral waves are self-sustained waves of excitation that rotate freely or around an obstacle, reactivating the same area of tissue at a higher frequency than normal, increasing the normal heartbeat rate (tachycardia). In the worst-case scenario, a spiral wave might break up into smaller spiral waves giving uncoordinated contractions of the heart in a phenomenon known as fibrillation. When this phenomenon occurs in the ventricles, the heart quivers and loses capacity to pump blood to the body leading to immediate cardiac arrest. Figure 10 shows the development of such a spiral wave on the same model as the one used for Figure 9. In this case, the spiral was triggered by adding a second stimulus at a certain location of the ventricle just after the normal wave had passed through this location. One can clearly see the spiral on the fringe components, and the reactivations of the pulse at higher frequencies on the potential vs time plot, where the chaotic dynamics can also be seen.

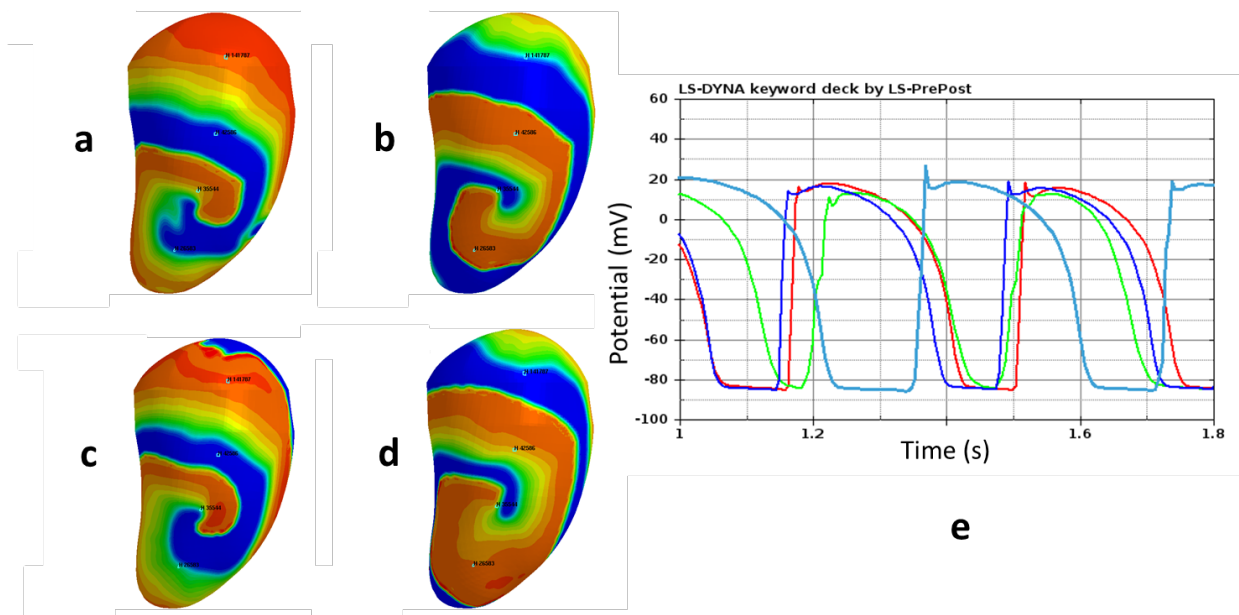


Figure 10: propagation of the transmembrane potential in a ventricle where a spiral wave has developed. The plots on the left show the fringe components of the potential at time 1050 ms (a), 1200 ms (b), 1400 ms (c), and 1600 ms (d). (e) shows time evolution of the potential at the 4 elements marked on the plots.

5- Purkinje network

The Purkinje network is a specialized conduction system within the heart that ensures the proper activation of the ventricles to produce effective contraction. During the ventricular contraction portion of the cardiac cycle, the Purkinje fibers carry the contraction impulse from both the left and right bundle branch to the myocardium of the ventricles. This causes the muscle tissue of the ventricles to contract and generate force to eject blood out of the heart, either to the pulmonary circulation from the right ventricle or to the systemic circulation from the left ventricle. The Purkinje network is thus an important part of the excitation system in the human heart, which is shown in figure 11. Yet, up to now, there is no in vivo imaging technique to accurately reconstruct its geometry and structure. Computational modeling of the Purkinje network is increasingly recognized as an alternative strategy to visualize, simulate, and understand the role of the Purkinje system.

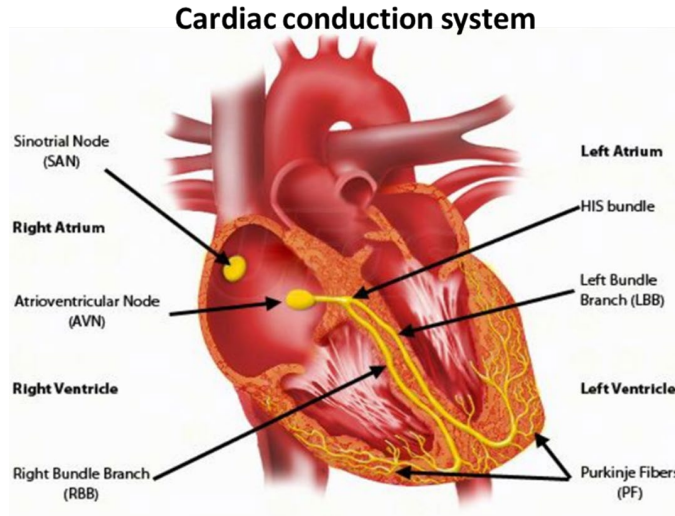


Figure 11: Cardiac conduction system showing the Purkinje fibers.

We thus developed an automatic 3D fractal network generation on a non-smooth surface (here, the endocardial surface of the ventricle), which is coupled to the 3D volume mesh, in a similar way as described in [14]. This Purkinje network is composed of conducting beams, and the leaves of the network are connected to the nodes of the volume mesh of the ventricle, thus allowing a coupling of the EP waves between the Purkinje network and the ventricles. Figure 12 shows such a network on a surface representing the endocardial surface of a ventricle, and figure 13 an EP wave propagation on a Purkinje network coupled with a ventricle.

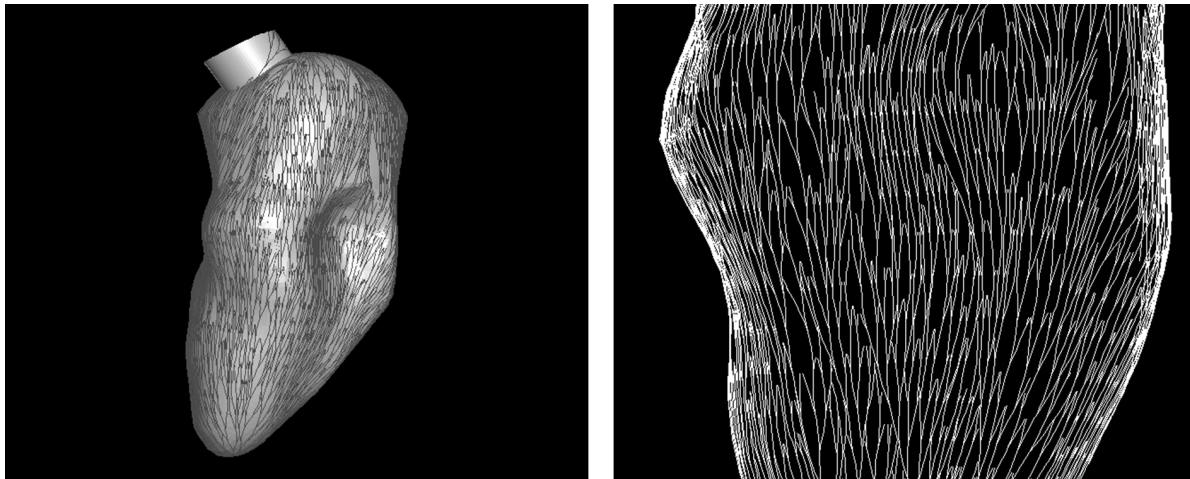


Figure 12: Automatically generated 3D fractal network of beams representing the Purkinje network generated on the endocardial surface of a ventricle (left) and zoom (right).

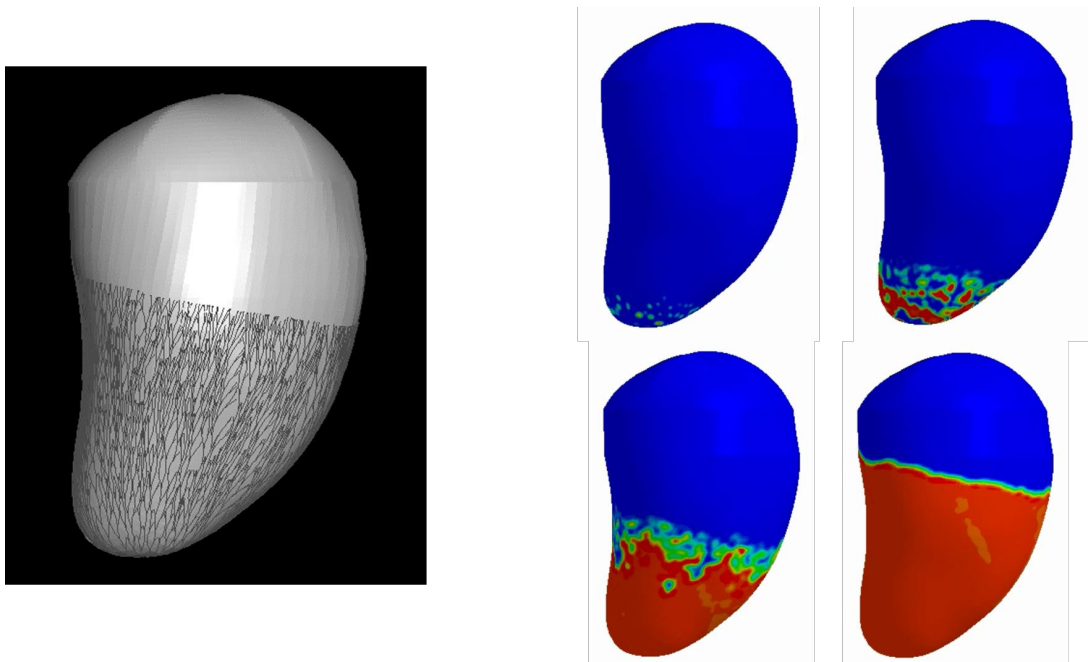


Figure 13: Propagation of the electric potential on the beam-made Purkinje fibers (left) coupled with the solid mesh representing the ventricle. The propagation is much faster in the Purkinje fibers than on the volume itself.

6-Coupling EP with the mechanics and FSI

The EP models give the local and temporal transmembrane potential as well as intracellular calcium ion concentration which provide the activation part of the heart muscle myofilament models, hence the input for the mechanical tissue models. A new anisotropic hyperelastic constitutive model, including an active term, *MAT_295, was developed in order to couple the EP with the mechanical deformations. These deformations can furthermore be coupled with the hemodynamics using the fluid-structure interaction (FSI) capabilities of the ICFD module of LS-DYNA. Figure 14 shows an example of a coupled EP-mechanics-FSI simulation.

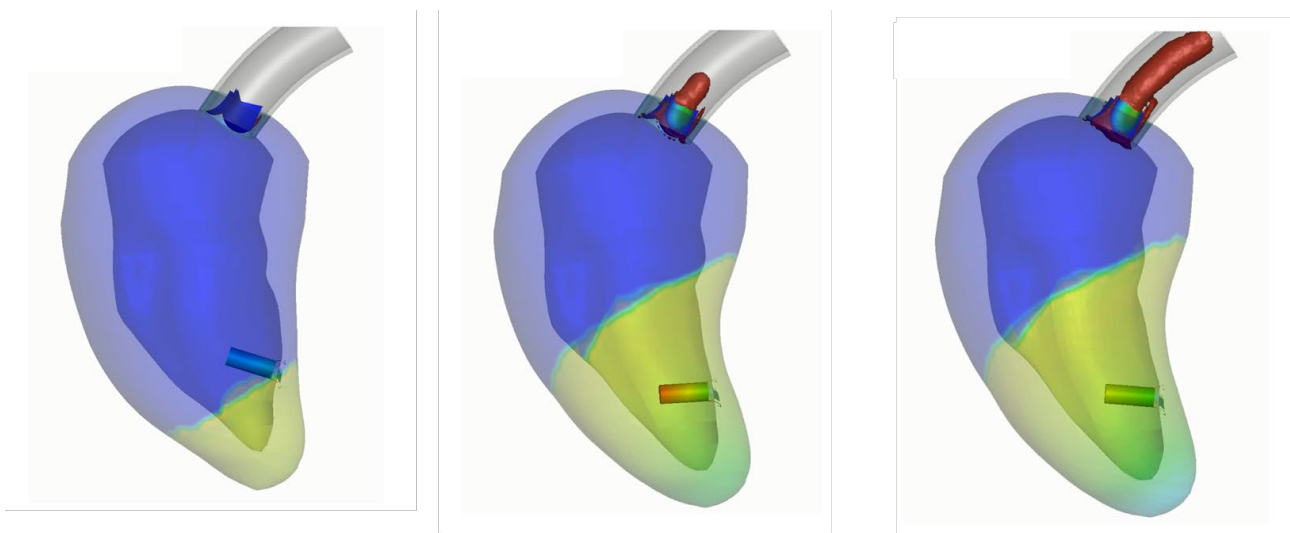


Figure 14: Ventricular contraction showing the propagation of the EP wave, the contraction of the ventricle, and the blood flow through the valve

Conclusion

An EP solver was introduced in LS-DYNA. Both monodomain and bidomain methods have been developed, with different algorithms for each of them. The 2 models can be coupled together in the same simulation and a surrounding bath can also be added. The mono and bidomain model models can be coupled to different cell models, including FitzHugh-Nagumo, Fenton-Karma, ten Tusscher and Panfilov, and a user-defined model. The model was compared to different benchmark cases, including one proposed by the FDA and shows good agreement with the other codes. The mono and bi-domain models can also be coupled with a Purkinje network which can be automatically generated on the endocardial surface of the ventricle.

Our goal is to be able to simulate a full heart beat, so the EP solver can be coupled with a new anisotropic hyperelastic constitutive model so that the EP wave can generate the deformation of the ventricles or atria which in turn can be coupled with the ICFD module to solve the hemodynamics part of the problem.

References

- [1] Ruth Aris Sanchez, Electromechanical Large Scale Computational Models of the Ventricular Myocardium, PhD Thesis, Universitat Politècnica de Catalunya, Sept. 2014.
- [2] Mark Potse, Bruno Dubé, Jacques Richer, Alain Vinet, and Ramesh M. Gulrajani, A Comparison of Monodomain and Bidomain Reaction-Diffusion Models for Action Potential Propagation in the Human Heart, *IEEE Trans. Biomed. Eng.*, vol. 53, no. 12, 2006.
- [3] FitzHugh R. Mathematical models of threshold phenomena in the nerve membrane. *Bull. Math. Biophysics*, 17:257–278, 1955
- [4] Nagumo J., Arimoto S., and Yoshizawa S. An active pulse transmission line simulating nerve axon. *Proc IRE*. 50:2061–2070, 1962
- [5] Fenton FH, Karma A., Vortex dynamics in three-dimensional continuous myocardium. Filament instability and fibrillation. *Chaos* 8: 20-47, 1998
- [6] K. H., W. J., ten Tusscher, A.V. Panfilov, Alternans and spiral breakup in a human ventricular tissue model, *Am. J. Physiol. Heart Circ., Physiol* 291: H1088-H1100, 2006.
- [7] M.E. Marsh, S.T. Ziaratgahi, and R.J. Spiteri, The secrets to the success of the Rush-Larsen method and its generalizations, *IEEE Trans. Biomed. Engrg.*, 59(9):2506-2515., 2015
- [8] Steven A. Niederer, Eric Kerfoot, Alan P. Benson, Miguel O. Bernabeu, Olivier Bernus, Chris Bradley, Elizabeth M. Cherry, Richard Clayton, Flavio H. Fenton, Alan Garny, Elvio Heidenreich, Sander Land, Mary Maleckar, Pras Pathmanathan, G. Plank, J. F. Rodriguez, I. Roy, F. B. Sachse, G. Seemann, O. Skavhaug, N. P. Smith, “Verification of cardiac tissue electrophysiology simulators using a N-version benchmark”, *Philosophical Transactions of the Royal Society A: Mathematical, Physical and Engineering Sciences*, vol. 369, issue 1954, pp. 4331-4351, November 2011.
- [9] Gernot Plank, Lufang Zhou, Joseph L. Greenstein, Sonia Cortassa, Raimond L. Winslow, Brian O'Rourke, Natalia A. Trayanova, From mitochondrial ion channels to arrhythmias in the heart: computational techniques to bridge the spatio-temporal scales, *Philos Trans A Math Phys Eng Sci*, 366(1879):3381-3409, September 2008.
- [10] Qu Z. and Garfinkel A., An advanced algorithm for solving partial differential equation in cardiac conduction, *IEEE Trans. Biomed. Eng.* 46:1166-1168, 1999
- [11] Hankarjee Krishnamoorthi, Mainak Sarkar, William S. Klug, Numerical Quadrature and Operator Splitting in Finit Element Methods to Cardiac Electrophysiology, *Int J Numer Method Biomed Eng.*, 29(11):1243-1266, November 2013.
- [12] Pathmanathan P., and Gray R., 2014, “Verification of computational models of cardiac electro-physiology”, *International Journal for Numerical Methods in Biomedical Engineering* 30:525-544
- [13] P. L'Éplattenier, S. Bateau-Meyer, D. Benson, V. Kaul, C. Schu, M. Palmer, D. Swenson, J. Blauer, “Cardiac simulations using LS-DYNA”, *Proc of the 15th LS-DYNA Users Conference*, Dearborn, 2018.
- [14] F.S. Costabal & Al, *J Biomech*, “Generating Purkinje Networks in the Human Heart” 2016 August 16; 49(12): 2455–2465.
- [15] M.J Bishop and G. Plank, “Representing Cardiac Bidomain Bath-Loading Effects by an Augmented Monodomain Approach: Application to Complex Ventricular Models”, *IEEE Trans Biomed Eng.* 2011 April, 58(4):1066-1075
- [16]. Vigmond E, Hughes M, Plank G, Leon L. “Computational tools for modeling electrical activity in cardiac tissue”. *J Electrocardiol.* 2003; 36:69–74. [PubMed: 14716595]
- [17] Mirams G, Arthurs C, Bernabeu M, Bordas R, Cooper J, Corrias A, Davit Y, Dunn S-J, Fletcher A, Harvey D, Marsh M, Osborne J, Pathmanathan P, Pitt-Francis J, Southern J, Zemzemi N, Gavaghan D. “Chaste: an open source C++ library for computational physiology and biology”. *PLoS Computational Biology* 2013; 9(3):e1002790.